IEEE Access
Multidisciplinary | Rapid Review | Open Access Journal

Received January 13, 2021, accepted January 26, 2021, date of publication February 5, 2021, date of current version February 12, 2021.

Digital Object Identifier 10.1109/ACCESS.2021.3057494

A Prediction Model Based on Artificial Neural Network for the Temperature Performance of a Hydrodynamic Retarder in Constant-Torque Braking Process

ZHUO WANG[1,2], WEI WEI[1,2,3], REZA LANGARI[4], (Senior Member, IEEE), QINGYU ZHANG[4], AND QINGDONG YAN[1,2]

[1]School of Mechanical Engineering, Beijing Institute of Technology, Beijing 100081, China
[2]National Key Laboratory of Vehicular Transmission, Beijing Institute of Technology, Beijing 100081, China
[3]Beijing Institute of Technology Chongqing Innovation Center, Chongqing 401120, China
[4]Department of Mechanical Engineering, Texas A&M University, College Station, TX 77840, USA

Corresponding author: Wei Wei (weiweibit@bit.edu.cn)

This work was supported in part by the National Natural Science Foundation of China under Grant 51475041 and Grant 51805027, and in part by the Beijing Institute of Technology Joint Ph.D. Student Training Scholarship.

ABSTRACT Excessively high brake temperature of hydrodynamic retarders may lead to brake fading and failure, resulting in a decrease in brake effectiveness. However, the temperature performance modeling of hydrodynamic retarders is a challenge because of the non-linear characteristics of the system. In this study, a temperature model based on an artificial neural network is constructed to predict the temperature performance of a hydrodynamic retarder in constant-torque braking process. The model is developed from a back-propagation neural network trained with the Levenberg-Marquardt algorithm. Before the application of the neural network, computational fluid dynamics is used to obtain the controllable region where experimental tests were performed to collect data for neural network training and validation. The linear regression method is adopted to check the quality of the training. It is shown that the constructed back-propagation neural network model is within 98% accuracy. Furthermore, the temperature model of the hydrodynamic retarder, which consists of the back-propagation neural network and thermal balance models, is simulated for 1500N·m, 2000N·m, and 2500N·m constant-torque braking processes. The simulation results are in agreement with experimental data within 2.87% error. The proposed temperature model can predict the temperature of the hydrodynamic retarder accurately and provide theoretical guidance for brake control strategy and thermal management.

INDEX TERMS Hydrodynamic retarder, back-propagation neural network, constant-torque braking, temperature performance.

I. INTRODUCTION

Hydrodynamic retarder is an effective auxiliary brake widely used on heavy-duty vehicles, featuring high braking torques, low unit weight, and good thermal decay characteristics compared with other auxiliary braking devices [1]. One of the important functions of hydrodynamic retarders is that it can provide constant braking torque for the vehicle driving downhill according to the driver's intention. Hydrodynamic retarder converts mechanical energy into liquid heat, resulting in efficient generation of braking torque. Heat energy emits into the environment by the heat exchanger and the shell of hydrodynamic retarder [2]. Although the working oil of hydrodynamic retarders is constantly cooled by cooling systems, the internal temperature of the retarder working chamber can reach a high level during long braking. When the temperature exceeds the maximum acceptable temperature, the hydrodynamic retarder downshifts automatically, and the total braking torque is reduced [3]. The temperature prediction model for hydrodynamic retarders enables the driver or the control system to take necessary emergency measures to avoid traffic accidents and can also serve as a

The associate editor coordinating the review of this manuscript and approving it for publication was Mark Kok Yew Ng.

reference for the cooling control system to adjust the coolant flow and to reduce unnecessary energy consumption.

Many studies have been conducted in the field of hydrodynamic retarder thermal properties. Wang *et al*. [4] established a hydraulic retarder cooling system model based on the Rankine cycle and analyzed its characteristics and power consumption under different working conditions. In this work, hydraulic retarder is simplified to a system composed of a heat source and a pump. Zhang *et al*. [5] designed a waste heat recovery system based on the Rankine Cycle. This system recycles waste heat energy in the transmission fluid to supplement the energy requirements for the cooling system. Liu *et al*. [6] combined computational fluid dynamic (CFD) simulation and multi-objective optimization to optimize the shape of the plate-fin heat exchanger for the hydraulic retarder. The internal flow fields involving temperature, pressure, and velocity were qualitatively compared to further emphasize the optimization effect. Liu *et al*. [7] developed an integrated cooling evaporation system for the hydraulic retarder which has a 200% heat-sinking capacity comparing to traditional plate-fin heat exchangers. The flow model and the heat source model of the transmission medium in the hydraulic retarder are established according to the traditional one-dimensional beam theory. Bu *et al*. [8] provided a comprehensive analysis of the thermophysical properties of the working oil in a hydraulic retarder and concluded that braking torque could increase with the enlargement of density and reduction of viscosity, while the specific heat and thermal conductivity have no obvious effect on braking performance. Zheng *et al*. [9] deduced a braking torque model by using fluid mechanics and a temperature rise model by using thermodynamics. The mathematical models can be used to describe the energy conversion of the hydraulic retarder. However, the temperature performance of hydrodynamic retarders is rarely reported, and its modeling approach needs to be studied.

Based on the literature review, CFD is one of the most used conventional methods for modeling the temperature of hydrodynamic retarders. It can make comprehensive quantitative and qualitative evaluation of internal flow field of hydrodynamic retarders, which is not easily obtained in experimental research [10]. However, the existing CFD models do not take into account the influence of the hydraulic control system on the internal flow field, which would reduce model accuracy. In addition, its input variable, namely charging rate, is difficult to measure during test. Also, the process of using CFD to learn the characteristic parameters of hydrodynamic retarder mechanism under all operation conditions is characterized by large computational load, long computational time, and high cost.

Estimation of hydrodynamic retarder temperature during braking process is a complex question characterized by a number of interacting factors between which the relationship is not precisely known. The artificial neural network (ANN) can establish the relationship between the input and output variables for non-linear and multi-dimensional systems without the knowledge of basic mechanism or complex mathematical equations [11]. In recent years, ANN has been extensively used for various disciplines [12]–[14]. Esfe *et al*. [15] predicted the thermal conductivity of nanofluids using ANN and nonlinear regression. The results show that the ANN model has good ability to predict the thermal conductivity of the nanofluids. Lin *et al*. [16] developed a deep belief network model to predict the stress of Ni-based superalloy. The results show that the deep belief network model can effectively characterize the hot deformation behavior of the Ni-based superalloy and has an excellent interpolation ability. Çay *et al*. [17] used an ANN model to predict the brake specific fuel consumption, effective power, average effective pressure, and exhaust gas temperature of a methanol engine. Results show that the ANN provided great accuracy in modeling the methanol engine performance. Therefore, ANN is a promising option for the temperature performance modeling of hydrodynamic retarders, if provided with sufficient experimental data, appropriate learning algorithms and network structures [18]. Among variety types of ANN models being selected for modeling hydrodynamic retarders, back-propagation neural network (BPNN) has been proven to be one of the most robust designs capable of producing fast and accurate fitting results. Yan [19] built the feedback oil pressure model of the hydraulic retarder based on BPNN and inspected its extrapolation ability. However, most scholars train the BPNN model based on the physical limits of the inputs instead of the controllable region of hydrodynamic retarders, which will increase the complexity and reduce the accuracy of temperature prediction model.

To the best of the authors' knowledge, this is the first study to investigate the temperature performance of a hydrodynamic retarder based on controllable region using ANN. In this study, a temperature model was developed to predict the temperature of a hydrodynamic retarder in constant torque brake process based on limited experimental data. Firstly, the controllable region was obtained with CFD. Secondly, the steady-state experiment of the hydrodynamic retarder was performed under several typical working conditions, and the data based on the controllable region were collected for subsequent network training and validation. Then, the BPNN was trained with the test data and was combined with the thermal balance model to constitute the temperature model of the hydrodynamic retarder. Finally, the temperature performance under various constant-torque braking processes was simulated, and its capability and accuracy were validated by experiment. This method can provide theoretical guidance for brake control strategy and thermal management.

II. SYSTEM DESCRIPTION

The entire hydrodynamic retarder is composed of three parts, hydrodynamic retarder working chamber, hydraulic system, and electronic control unit (ECU) as shown in Fig. 1. The working chamber is constituted by a rotor and a stator with an inlet and an outlet. The braking control strategy is stored in the ECU. When the hydrodynamic retarder starts working,

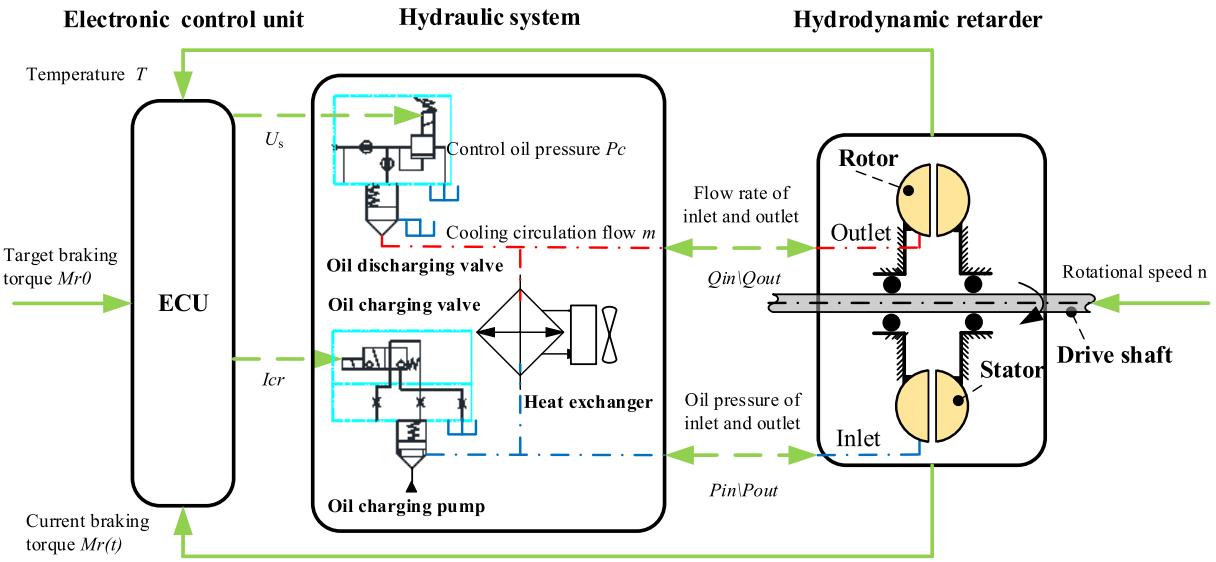

FIGURE 1. Structure and working principle of the entire hydrodynamic retarder.

the ECU outputs control signals to open the oil charging valve and regulates the control oil pressure of the oil discharging valve. Then the working oil flows from the oil charging pump into the working chamber. The rotor drives the working oil to circulate in the working chamber so that braking torque is generated by a reaction force between the rotor and the stator. After that, the working oil enters the oil discharging valve through the outlet. At the same time, the control oil pressure of the oil discharging valve adjusts both the charging rate of the working chamber and the cooling circulation flow, which is cooled by the heat exchanger before flowing back to the working chamber [20]. Meanwhile, the ECU records the target braking torque according to drivers' intention, and collects the current braking torque and temperature in a timely manner. When the hydrodynamic retarder stops working, the ECU outputs the control signals to close the oil charging valve and to fully open the oil discharging valve, which makes the working oil flow from the working chamber back into the tank. At this time, the charging rate is nearly zero.

III. TEMPERATURE MODEL

The hydrodynamic retarder temperature model consists of two sub-models (Fig.10): one is the BPNN model and the other is the thermal balance model. The BPNN model builds the relationship between the inputs (control oil pressure and rotational speed) and the outputs (braking torque and cooling circulation flow) of the hydrodynamic retarder. The thermal balance model involves the heat generation from braking torque and hydraulic power, the heat loss via the cooling system, and the heat loss to the ambient air. These two models together have effects on the temperature rise in the braking process.

A. CONTROLLABLE REGION

When the control oil pressure is above the upper threshold or below the lower threshold, the oil discharging valve is fully closed or fully open, and the braking torque is maximized or minimized. Therefore, there is a controllable region beyond which the control oil pressure can change neither the opening degree of the oil discharging valve nor the braking torque. To decrease the complexity of the model, the uncontrollable region is ignored in the sequel. While the boundary of the controllable region of the control oil pressure is determined by the rotational speed, the boundary of the rotational speed is affected by the power of the electrical motor. Since the controllable region could not be obtained in the experimental study, it is determined by simulation before the study.

The outlet oil pressure of the hydrodynamic retarder at maximal and minimal charging rate at different rotor rotational speeds was simulated by CFD [21]. Here are the assumptions and conditions of the simulation. The oil is assumed to be an incompressible viscous fluid, and its density and viscosity are determined by the temperature of the working chamber, which can be calculated according to [22]. It is also assumed that there is no leakage in the working chamber and no deformation of flow passage caused by fluid–solid interaction between the working fluid and the impeller. Boundary conditions were set according to the working conditions of the hydrodynamic retarder. The inlet part was set as the velocity inlet, which defined the flow rate through the hydrodynamic retarder (as the flow rate in the experiment is determined by the oil charging pump). The pressure of the outlet was defined by the standard atmospheric pressure. Other surfaces were assumed to be rigid walls with no slip in the steady-state simulation. Finite volume method was used to discretize the control equations. The standard $k-\varepsilon$ model was used as the turbulence model [23]. The main parameters of the hydrodynamic retarder are listed in Table 1. The CFD model of the hydrodynamic retarder with inlet and outlet is shown in Fig. 2. In the conditions of maximal and minimal charging rate, the outlet pressure p_{out} of

TABLE 1. Main parameters of hydrodynamic retarder.

Parameters	Rotor/Stator
External diameter	380 mm
Internal diameter	220 mm
Blade number	20/24
Blade thickness	4 mm
Blade angle	30°

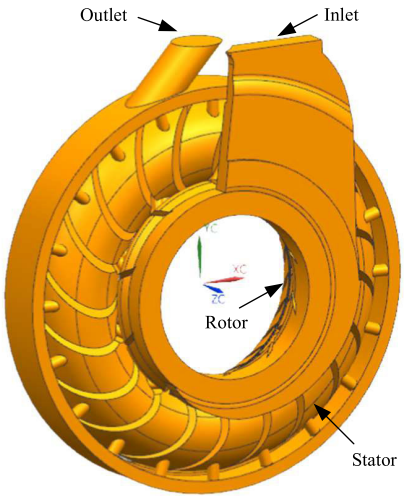

FIGURE 2. CFD model of hydrodynamic retarder with inlet and outlet.

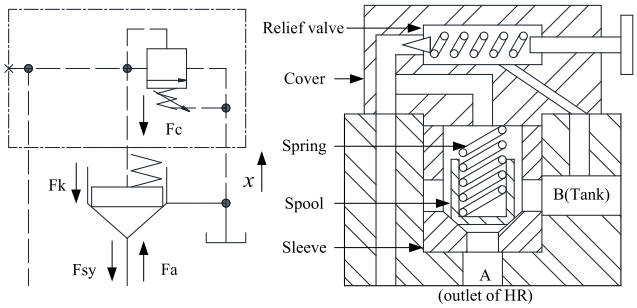

FIGURE 3. Schematic diagram of oil discharging valve.

the hydrodynamic retarder at different rotational speeds was simulated.

Fig. 3 shows a schematic diagram of the oil discharging valve. Port A is connected to the outlet of the hydrodynamic retarder and the inlet of heat exchanger while port B is always connected to the tank. The valve is composed of a relief valve regulating control force, a cover connecting the pressure relief valve and valve body, a main spool, a sleeve containing the main spool, and a spring [24].

When there is no liquid flow in the damping hole of the oil discharging valve, the spool weight and viscous friction were ignored [25]. The maximal and minimal control oil pressure at different rotational speeds were calculated in Fig. 4 based on the CFD simulation results using the spool force balance equation (1):

$$F_c - F_a + F_k + F_{sy} = 0 \tag{1}$$

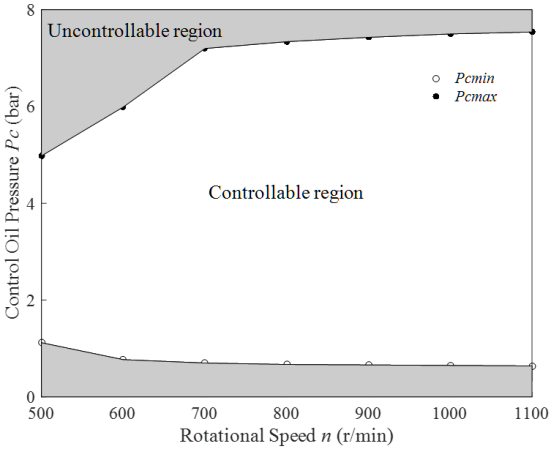

FIGURE 4. The maximal and minimal control oil pressure of the controllable region at different rotational speeds.

where $F_c = \frac{\pi}{4}D_c^2 P_c$ is the control force generated by the control oil pressure, P_c is the pressure of the control oil, D_c is the diameter of the cavity hole of the control chamber, $F_a = \frac{\pi}{4}D_a^2 P_a$ is the force on the acting face of the inlet, P_a is the inlet pressure of the oil discharging valve which is assumed equal to P_{out}, D_a is the diameter of the inlet of the oil discharging valve, $F_k = K(X_0 + X)$ is the reset stretch, K is the reset spring stiffness, X_0 is the initial compression of the reset spring, F_{sy} is the steady flow force.

B. EXPERIMENTAL TESTING

The experimental equipment is mainly composed of power source (electrical motor), inertia device, torque and rotational speed sensors, and hydrodynamic retarder, connected by couplings. The experimental equipment and arrangement are shown in Fig. 5. The technical specifications of the test are given in Table 2. Parameters measured in this study and their range and accuracy are listed in Table 3.

TABLE 2. The technical specifications of the test system.

Parameters	Values
Motor rated power	630 kW
Motor rated speed	3000 r/min
Inertia	45 kg·m^2
Cooling water flow	252 m^3/h
Heat dissipation area	44 m^2/h
Ambient temperature	25°C

TABLE 3. Range and accuracy of the parameters measured.

Parameters	Range	Accuracy
Rotational speed	0-10000 r/min	± 0.1%
Torque	0-5000 N·m	± 0.1%
Pressure	0-16 bar	± 0.5%
Flow	30-330 L/min	± 3%
Temperature	-30-150°C	± 1%

The steady-state tests were conducted after the hydrodynamic retarder runs fully and stably. The range of the rotational speed of the tests is from 500 r/min to 1100 r/min. Such

TABLE 4. Experimental test results to obtain braking torque and cooling circulation flow.

Sample no.	Rotational speed (r/min)	Control oil pressure (bar)	Braking torque (N·m)	Cooling circulation flow (L/min)	Sample no.	Rotational speed (r/min)	Control oil pressure (bar)	Braking torque (N·m)	Cooling circulation flow (L/min)
1	**500**	**1.12**	**835.3**	**55.5**	28	800	7	3748.2	167.6
2	500	1.5	1035.5	65.9	**29**	**800**	**7.2**	**3790.3**	**167.8**
3	500	3	1212.2	74.1	**30**	**900**	**0.66**	**534.6**	**50.3**
4	500	4	1265	75.8	31	900	1.5	987.1	84.5
5	500	5	1276.4	76.1	32	900	3	1805.1	128.5
6	**500**	**5.2**	**1277.9**	**76.2**	33	900	4	2519.1	155.7
7	**600**	**0.77**	**731.2**	**54.6**	34	900	5	3229.1	174.9
8	600	1.5	1076.8	76.6	35	900	6	3793.8	189.2
9	600	3	1603.2	98.6	36	900	7	4264.2	194
10	600	4	1918.7	108.3	**37**	**900**	**7.3**	**4339.7**	**194.5**
11	600	5	2086.5	110.7	**38**	**1000**	**0.65**	**524.9**	**49.8**
12	600	6	2159.1	111.1	39	1000	1.5	959.8	72.1
13	**600**	**6.1**	**2165**	**111.3**	40	1000	3	1844.3	134.3
14	**700**	**0.7**	**660.7**	52.4	41	1000	4	2678.3	161.2
15	700	1.5	1168.2	89.2	42	1000	5	3412	186.4
16	700	3	1878.2	125.7	43	1000	6	4189	202.8
17	700	4	2363	133.2	44	1000	7	4496.3	208.5
18	700	5	2694.3	137.3	**45**	**1000**	**7.4**	**4541.6**	**209.4**
19	700	6	2965.4	141.1	**46**	**1100**	**0.64**	**511.3**	**49.3**
20	700	7	3135.3	141.6	47	1100	1.5	1000.9	82.4
21	**700**	**7.1**	**3156**	**141.7**	48	1100	3	1777.1	133.9
22	**800**	**0.67**	**592.7**	**51.8**	49	1100	4	2584.3	164.6
23	800	1.5	1193.1	85.2	50	1100	5	3443.7	192.6
24	800	3	1895.9	126.2	51	1100	6	4204.5	212.8
25	800	4	2499.7	145.1	52	1100	7	4747.5	219.7
26	800	5	3057.5	159.5	**53**	**1100**	**7.5**	**4905.9**	**220.8**
27	800	6	3485.9	166.1					

The bold values are the boundary parameters of the controllable region.

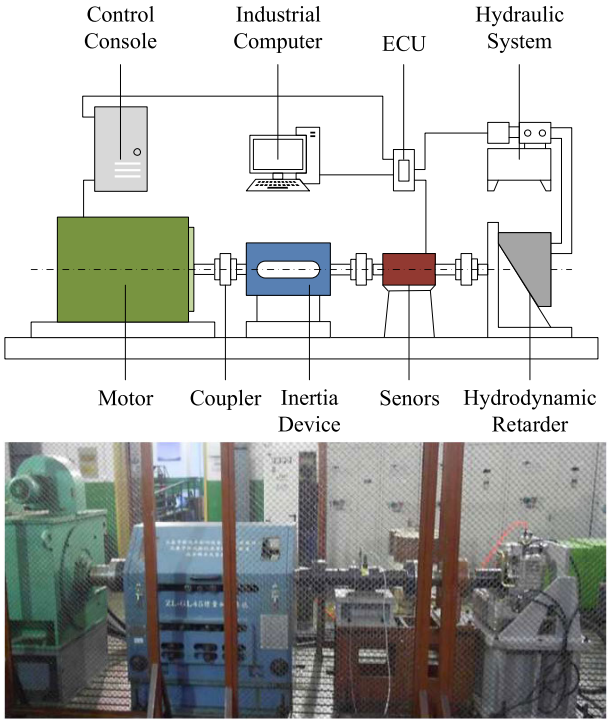

FIGURE 5. Experimental equipment and arrangement.

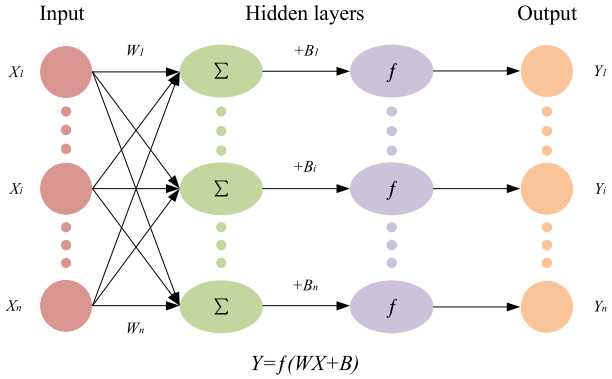

FIGURE 6. Typical structure of back-propagation neural network.

lower bound and upper bound are selected based on vehicle idle speed and motor power limit respectively. In steady-state test, the rotational speed was fixed but the control oil pressure was varied to obtain the braking torque at different control oil pressures. The test results were recorded through embedded programs in data acquisition system with at 50 Hz. According to the data structure of hydrodynamic retarder, 71 experimental data sets uniformly distributed over the controllable region were collected, of which 53 sets (nearly 75%) were used for training, as is shown in Table 4. The remaining 18 data sets (25%) were used for validation.

C. BACK-PROPAGATION NEURAL NETWORK

BPNN is a non-linear feedforward network using back-propagation algorithm to realize training target. Theoretically, the neural network with enough hidden layer and unit can approximate any non-linear relationship [12]. Fig. 6 shows the typical structure of a BPNN. The equation

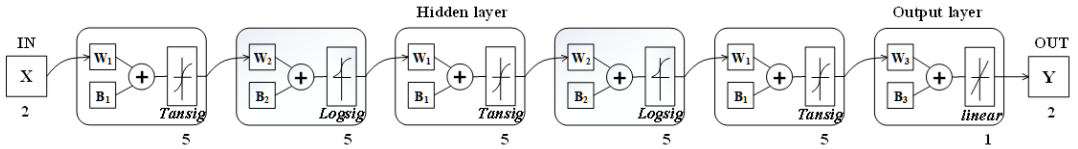

FIGURE 7. The structure of back-propagation neural network for modeling of braking torque and cooling circulation flow.

in Fig. 7 represents the mathematical relationship between the inputs X and the outputs Y, where f is the transfer function for hidden and output layers. This relationship can be established by adjusting the weight matrices W and bias vectors B in the hidden layers and the output layers to minimize the mean square error value during the training processes [26]. In this study, control oil pressure and rotational speed were selected as the inputs, while braking torque and cooling circulation flow were selected as the outputs. The design of BPNN also includes the transfer function, the number of layers, and the number of neurons of the hidden and the output layer [27].

The Sigmoid function is commonly used as the transfer function in the hidden layers for a BPNN. The shape of the Sigmoid function, steep in the middle and flat at the ends, is similar to the way neurons in the human brain work, which makes it suitable for test data fitting of the hydrodynamic retarder because of the low sensitivity to noisy data [28]. In addition, tangent (Tansig) $\varphi(x)$ and logarithmic (Logsig) $\psi(x)$ in (2) and (3) were used in this research as well [29].

$$\varphi(x) = \frac{2}{1+e^{-2x}} - 1 \tag{2}$$

$$\psi(x) = \frac{1}{1+e^{-x}} \tag{3}$$

For the output layer transfer function, the Sigmoid function appears to be inappropriate as it narrows the output signal to a sensitive range [30]. And the output layer should faithfully transfer the signal from the last hidden layer to the output layer. Therefore, a linear function was adopted [31].

The number of hidden layers and neurons have great influence on the performance of BPNN. The number of neurons in the hidden layer can be determined by the number of neurons in the input layer by Kolmogorov's theorem [32], as described in (4), where n_h and n_i are the number of neurons in the hidden layer and the input layer, respectively [33]. In this study, n_i is set as 2, and n_h is 5 consequently.

$$n_h = 2n_i + 1 \tag{4}$$

The performance of the BPNN model was evaluated statistically using three prediction score metrics, namely the coefficient of correlation (R^2) [34], root-mean-square error ($RMSE$) [35], and Nash–Sutcliffe efficiency coefficient (NSE) [36] in the following equations:

$$R^2 = \frac{\sum_{i=1}^{n}(f_{EXP,i} - \bar{f}_{EXP})(f_{BPNN,i} - \bar{f}_{BPNN})}{\sqrt{\sum_{i=1}^{n}(f_{EXP,i} - \bar{f}_{EXP})^2 (f_{BPNN,i} - \bar{f}_{BPNN})^2}} \tag{5}$$

$$RMSE = \sqrt{\frac{\sum_{i=1}^{n}(f_{EXP,i} - f_{BPNN,i})^2}{n}} \tag{6}$$

$$NSE = 1 - \sum_{i=1}^{n} \frac{(f_{EXP,i} - f_{BPNN,i})^2}{(f_{EXP,i} - \bar{f}_{EXP,i})^2} \tag{7}$$

where $\bar{f}_{EXP} = \frac{1}{n}\sum_{i=1}^{n} f_{EXP,i}$, $\bar{f}_{BPNN} = \frac{1}{n}\sum_{i=1}^{n} f_{BPNN}$, n is the number of data sets used for training, f_{EXP} is the output obtained from the experiment, f_{BPNN} is the output predicted by the network.

As there are no fixed rules in determining the BPNN structure or its parameter values, several networks of different numbers and transfer functions of hidden layers were trained until an acceptable error was obtained, namely the highest R^2, NSE and the lowest $RMSE$. Comparison of different trained networks are shown in Table 5. By trial and error, the best prediction accuracy occurs when there are 5 hidden layers whose transfer functions are Tansig, Logsig, Tansig, Logsig, Tansig, as shown in Fig. 7.

Fig. 8 shows the linear regression relationship between the model output (Mro, qo) and the corresponding target ($Mrct$, qct), which are used to verify the training quality of the model. Here Mro and qo are the braking torque and the cooling circulation flow output by the BPNN, $Mrct$ and qct are the experimental values of the braking torque and the cooling circulation flow. The ideal fit is shown as dashed lines ($Mro = Mrct, qo = qct$) where outputs are equal to targets. Two regression lines (green solid lines in the figure) are computed to approximate the output data (hollow circles in the figure). 1.0041, 1.0008 and 0.3574, 1.1433 correspond to the slope and the y-intercept of the regression lines. In other words, the regression lines and the ideal fitting lines almost overlap. In conclusion, the model is of excellent training quality [37].

After training, the network was tested. In this way, a higher generalization level can be guaranteed. The model outputs, braking torque and cooling circulation flow, are shown in Fig. 9 (a) and (b). The testing accuracies for Mr and q were above 98% and 99% according to Fig. 9 (c) and (d). It proves that the developed hydrodynamic retarder model has excellent interpolation ability and can provide reliable data.

A larger network almost invariably achieves a low error eventually, but this may indicate overfitting rather than a good model. An overfitted model can be easily diagnosed by monitoring the performance of the model during training.

TABLE 5. Comparison of trained networks for braking torque.

Serial no.	Layer structure	Hidden transfer function	R^2	$RSME$	NSE
1	$2\times5\times5\times5\times5\times2$	Tansig, Logsig, Tansig, Logsig	0.99995	0.58432	0.999999487
2	$\mathbf{2\times5\times5\times5\times5\times5\times2}$	**Tansig, Logsig, Tansig, Logsig, Tansig**	**0.99997**	**0.47809**	**0.999999878**
3	$2\times5\times5\times5\times5\times5\times2$	Logsig, Tansig, Logsig, Tansig, Logsig	0.99995	0.57071	0.999999272
4	$2\times5\times5\times5\times5\times5\times5\times2$	Logsig, Logsig, Logsig, Logsig, Logsig	0.99994	0.65356	0.999999091
5	$2\times5\times5\times5\times5\times5\times5\times2$	Tansig, Tansig, Tansig, Tansig, Tansig	0.99996	0.51130	0.999999506
6	$2\times5\times5\times5\times5\times5\times5\times2$	Tansig, Tansig, Logsig, Tansig, Tansig	0.99995	0.57321	0.999999358
7	$2\times5\times5\times5\times5\times5\times5\times2$	Logsig, Logsig, Tansig, Logsig, Logsig	0.99993	0.69591	0.999999656

The bold values are selected as parameters of the optimum structure.

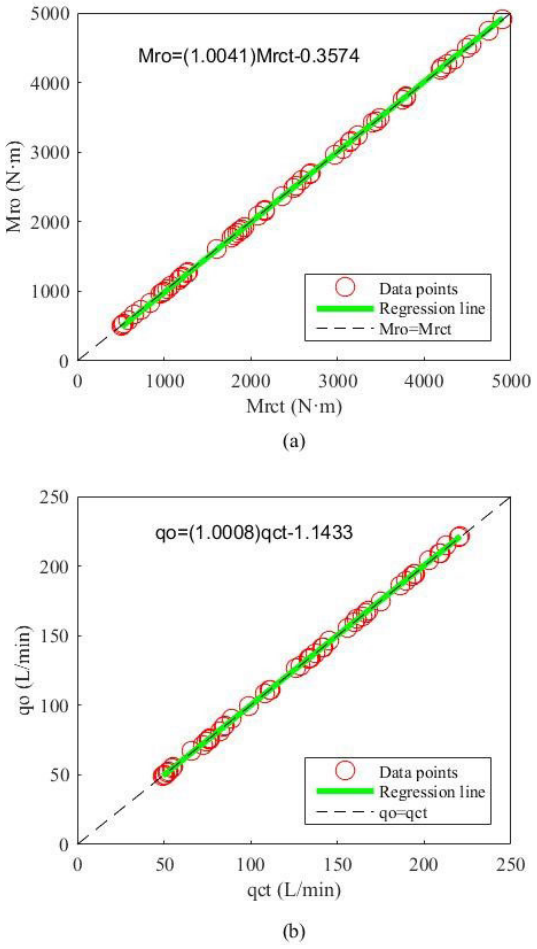

FIGURE 8. Linear regression relationship for modeling result and experimental data of braking torque and cooling circulation flow.

The accuracy on test data at the end of each epoch was computed, and training stopped when the accuracy was no more improving [38]. In this way, a perfect fit between underfitting and overfitting was obtained.

The time complexity for training a back-propagation neural network that has 5 layers is $O(nt*(ij+jk+kl+lm))$, where i, j, k, l, and m denote the number of nodes of the input layer, the second layer, the third layer, the fourth layer, and the output layer respectively, with t training examples and n epochs. Back-propagation can be expressed for simple feed-forward networks in terms of matrix multiplication. Each matrix size is determined by the nodes of two adjacent layers. The time complexity of matrix multiplication for $M_{ij}*M_{jk}$ is simply $O(i*j*k)$ [39]. For the back-propagation algorithm starting from the output layer $m\rightarrow l$, the time complexity is $O(m*t*l)$. Now going back from $l\rightarrow k$, the time complexity is $O(l*t(m+k))$. Using the same logic for $k\rightarrow j, j\rightarrow i$, the total time complexity for one epoch is $O(t*(ij+jk+kl+lm))$.

D. THERMAL BALANCE MODEL

The heat generation from braking power is spread throughout the working oil by means of conduction and causes the increase of temperature. The calorific capacity of the hydrodynamic retarder is expressed as follows:

$$Q_r=\frac{M_r n(1-\eta)}{9550} \tag{8}$$

where M_r is the braking torque (N·m), n is the rotational speed (r/min), η is the efficiency.

The hydraulic control system of hydrodynamic retarder is mainly composed of valves, oil charging pump, control oil pump, tank, and connecting pipes. When the working oil circulates in these components, pressure loss and flow loss such as valve's throttling loss and pump's volumetric loss inevitably occur. These power losses are eventually converted to heat energy absorbed by the working oil [40]. The calorific capacity of the hydraulic control system is expressed as follows:

$$Q_h=\frac{\Delta p q_h}{60} \tag{9}$$

where Δp is the differential pressure (Mpa), q_h is the flow (L/min).

The heat loss via the cooling system is mainly convection heat transfer. The heat dissipating capacity of the cooling system is expressed as follows [41]:

$$Q_c=K_r A_c \Delta t_m \tag{10}$$

where K_r is the convection heat transfer coefficient (W/m^2· K), A_c is the heat dissipation area of heat exchanger (m^2), $\Delta t_m=\frac{\Delta t_{max}-\Delta t_{min}}{ln\Delta t_{max}\backslash\Delta t_{min}}$ is the log mean temperature difference (K), Δt_{max} is the maximum temperature difference of the two fluids at each end of the heat exchanger, and Δt_{min} is the maximum temperature difference of the two fluids (K).

The heat loss from the hydrodynamic retarder shell to the ambient air are mainly convection heat transfer as well. The heat dissipating capacity of the hydrodynamic retarder shell

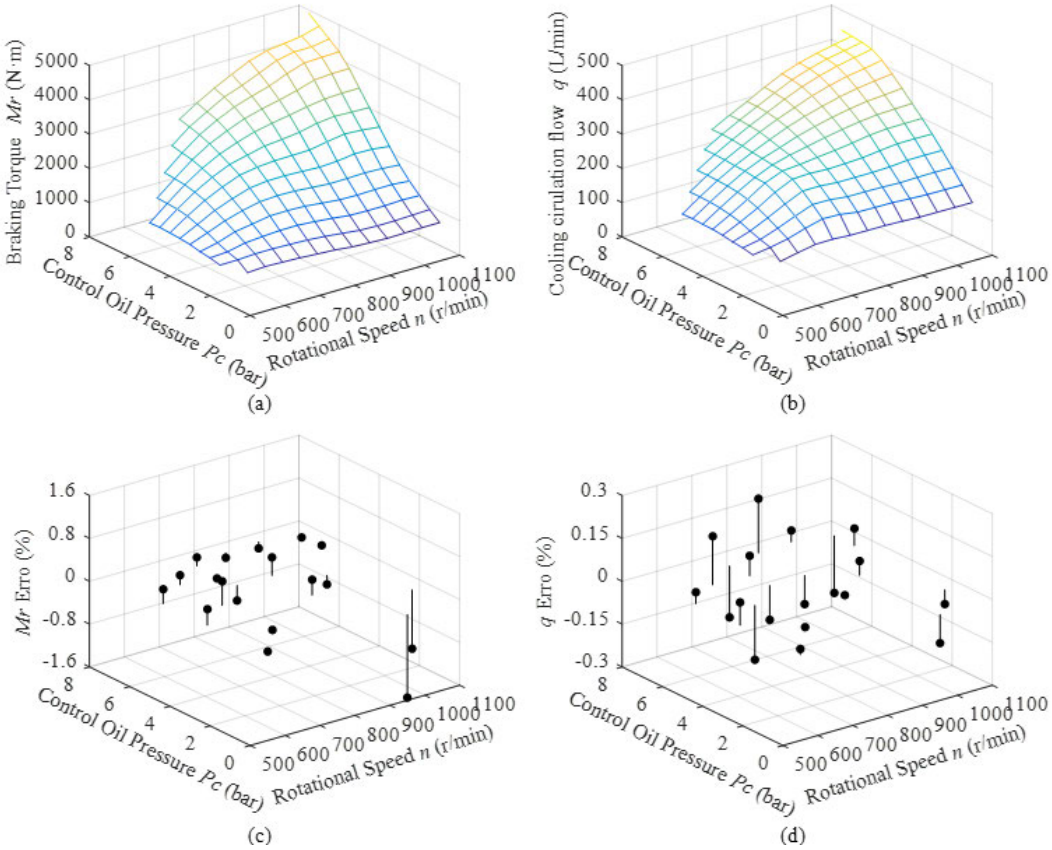

FIGURE 9. Linear regression relationship for modeling result and experimental data of braking torque and cooling circulation flow.

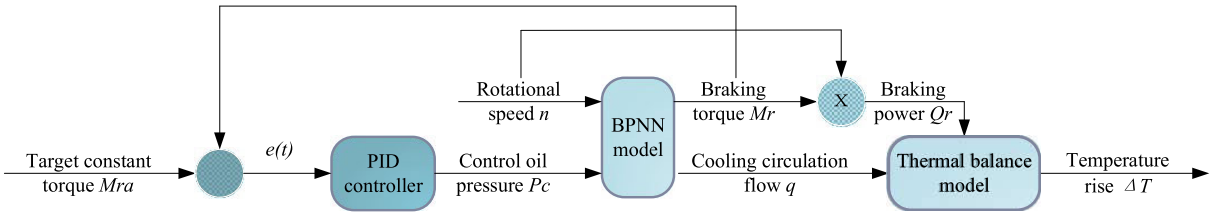

FIGURE 10. The block diagram structure of the constant-torque control system.

is expressed as follows:

$$Q_s = \frac{A_s q_s \delta}{2} \tag{11}$$

where A_s is the heat dissipation area of the shell (m^2), q_s is the heat transfer rate (W/m^3), δ is the wall thickness of the shell (m).

According to the energy balance, the temperature rise of the working oil in the hydrodynamic retarder is expressed as follows:

$$\frac{dT_O}{dt} = \frac{Q_r + Q_h - Q_c - Q_s}{C_o \dot{m}} \tag{12}$$

where C_O is the specific heat capacity of working oil (J/kg· K), $\dot{m} = q\rho$ is the mass flow rate (kg/s), q is the cooling circulation flow (L/min), ρ is the density of working oil (kg/m^3).

IV. TEMPERATURE PERFORMANCE

The target of brake control of the hydrodynamic retarder is to keep the braking torque constant under constant and varying rotational speed. In other words, the controller produces a proper control oil pressure so that the braking torque can remain constant. The block diagram of the constant torque control system is shown in Fig. 10. A proportional integral derivative (PID) controller is applied to closed-loop braking torque control under various rotational speed conditions, which has the advantages of fast response, high stability, easy parameters setting and low cost. The input of the controller is the error between the target braking torque and the actual braking torque, and the output is the control oil pressure signal. The effects of all three individual parameters (P-I-D) add up to produce the output. Manual tuning of PID parameters is applied in this study as a proper approach due

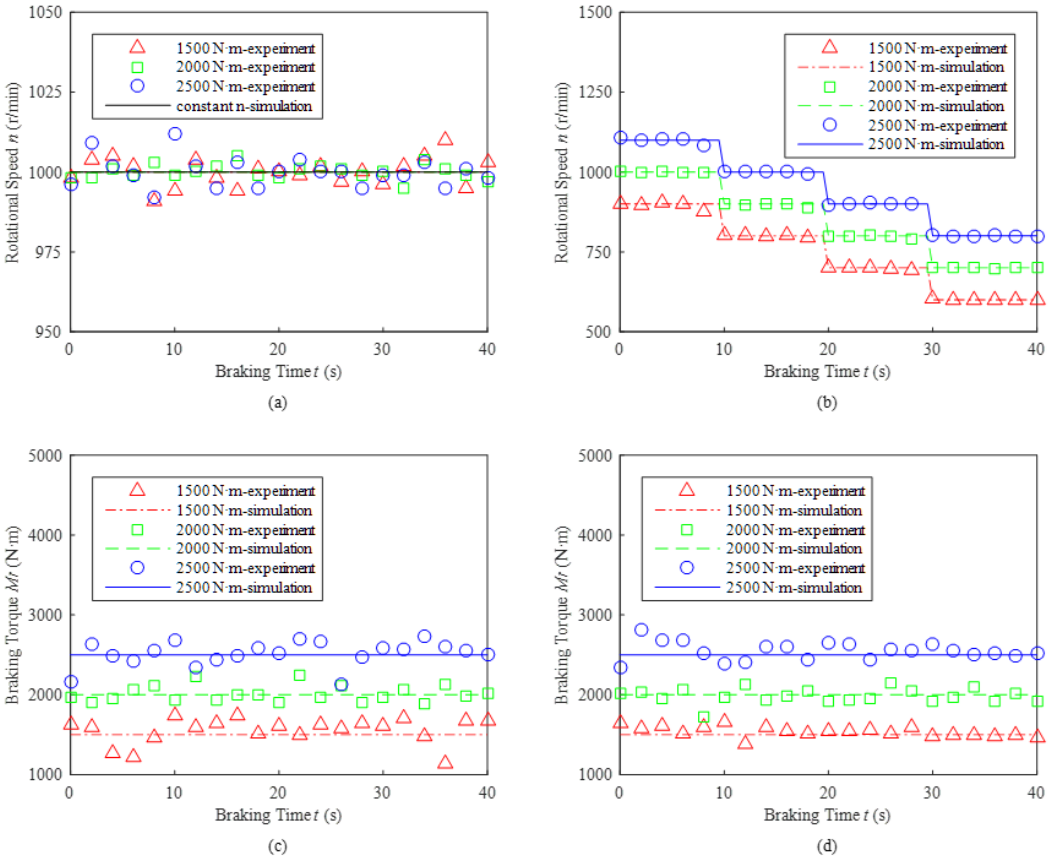

FIGURE 11. Simulation/Experiment comparison: constant braking torque under the constant and varying rotational speed.

to the fact that the constant-torque braking process is steady and free of noise [42].

An experimental study was conducted to validate the accuracy of temperature model. For the sake of safety, the experiment was carried out under initial temperature of 80°C and braking time of 40 s. Due to the limit of the engine power, the experiments were conducted at 1500 N·m, 2000 N·m, and 2500 N·m respectively, under constant and varying rotational speeds, as shown in Fig. 11 (a), (b), (c), (d). These operations were repeated for three times in the same method to insure that test results are reliable. Then the test rotor rotational speed and control parameters were used to temperature model. The comparison of the temperature data from simulation and experiment is shown in Fig. 12 (a), (b). Temperature errors between experiment and simulation are given in Fig. 12 (c) and (d), respectively. The relative error between the simulating results and the experimental data is defined as follows:

$$\delta = \frac{x_0 - x_t}{x_t} \times 100 \tag{13}$$

where x_0 and x_t are the values of the simulating results and the experimental data, respectively.

The temperature continues to increase in the constant-torque braking processes, as shown in Fig. 12 (a), (b). Since constant torque means braking power is also constant,

TABLE 6. The predicted and experimental temperature at the end of braking time, under constant and varying rotational speed.

Braking torque M_{ra} (N·m)	Rotational speed n (r/min)	Temperature T (°C) simulation/experiment
1500	1000	86.9°C/86.7°C
2000	1000	90.5°C/90.4°C
2500	1000	92.4°C/92.6°C
1500	900-600	92.1°C/92°C
2000	1000-700	98.9°C/99.1°C
2500	1100-800	103.7°C/103.5°C

the highest temperature appears at the end of the braking. The temperature rise rate could be determined from the constant-slope curve. The rise rates under constant rotational speed 1000 r/min are 0.172°C/s, 0.263°C/s, and 0.31°C/s for three constant torques. Under varying rotational speed, namely when braking power is varying, the rise rate of T will decrease with the reduction of rotational speed. The simulated and experimental temperature at the end of braking process under constant and varying rotational speed are shown in Table 6. Also, the results in Fig. 12 (c), (d) show that the simulated curves fits well with the experimental data, since the maximal temperature difference is 2.3°C. It is acceptable for prediction to have such a small error in comparison to the actual high working chamber temperature, considering the fact that the temperature is inevitably affected by system

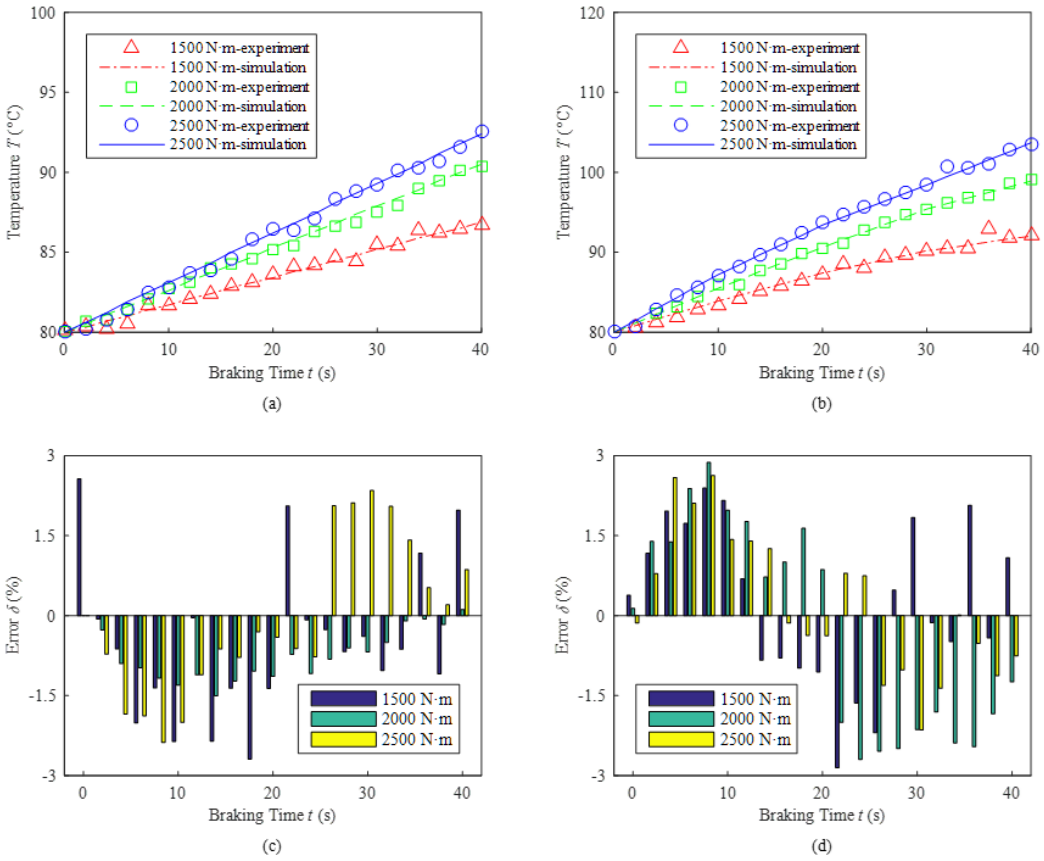

FIGURE 12. Simulation/Experiment comparison: temperature and its error in constant-torque braking process under the constant and varying rotational speed.

pressure oscillation, internal leakage, and temperature sensor delay.

In this study, a method is developed to predict temperature changes in braking process. Validation claims that the temperature prediction model is feasible. However, some limitations of this method can be expected. Though the prediction process runs fast, the training and test data have to be recollected, and the model has to be retrained if the type of hydrodynamic retarder is different. In addition, temperature prediction model based on BPNN essentially works as black box and cannot quantify the effect of each input on the network output.

V. CONCLUSION

Based on the experimental data, a temperature prediction model of a hydrodynamic retarder is developed. The optimized structure of back-propagation neural network model is 2-5-5-5-5-5-2, and its testing accuracy is 98%. It is found from the temperature performance curves that the temperature of hydrodynamic retarder is positively related to the braking power and the braking time, and the temperature rise rate is determined by the braking power. Furthermore, the output of the temperature model accords well with the experimental data within $\pm 2.87\%$ error. The high accuracy indicates that the developed temperature prediction model is able to effectively predict the temperature of the hydrodynamic retarder operating in the controllable region. The presented model also can provide technical references to matching design of the cooling system, brake control and thermal management of the hydrodynamic retarder.

REFERENCES

[1] H. Mu, J. Fu, Z. Wu, Y. Zhu, W. Wei, and Q. Yan, "Optimization on parallel control of PID and fuzzy in constant-speed braking process with a hydrodynamic retarder," in *Proc. IEEE 8th Int. Conf. Fluid Power Mechatronics (FPM)*, Apr. 2019, pp. 1175–1188.

[2] Z. Ji, Y. Li, R. Xi, and J. Jia, "Elastic-plastic analysis for wet multidisc brake during repeated braking," *Proc. Inst. Mech. Eng., C, J. Mech. Eng. Sci.*, vol. 230, no. 17, pp. 2968–2981, Oct. 2016.

[3] H. Zheng, Y. Lei, and P. Song, "Design of the filling-rate controller for water medium retarders on the basis of coolant circulation," *Proc. Inst. Mech. Eng., D, J. Automobile Eng.*, vol. 230, no. 9, pp. 1286–1296, Aug. 2016.

[4] T. Wang, G. Tan, X. Guo, S. Xiong, Z. Zhang, and X. Gao, "Energy saving analysis of vehicle hydraulic retarder thermal management system based on rankine cycle," SAE Tech. Paper 2016-01-1941, 2016.

[5] Z. Zhang, G. Tan, M. Yang, Z. Yang, and M. Han, "Experimental study of hydraulic retarder waste heat recovery based on the organic rankine cycle," SAE Tech. Paper 2016-01-8079, 2016.

[6] C. Liu, W. Bu, and D. Xu, "Multi-objective shape optimization of a plate-fin heat exchanger using CFD and multi-objective genetic algorithm," *Int. J. Heat Mass Transf.*, vol. 111, pp. 65–82, Aug. 2017.

[7] W. Liu, G. Tan, J. Li, X. Li, F. Mou, and Y. Ge, "Integrated cooling evaporation system for the hydraulic retarder," SAE Tech. Paper 2015-01-1612, 2015.

[8] W. Bu, G. Shen, H. Qiu, and C. Liu, "Investigation on the dynamic influence of thermophysical properties of transmission medium on the internal flow field for hydraulic retarder," *Int. J. Heat Mass Transf.*, vol. 126, pp. 1367–1376, Nov. 2018.
[9] H. Zheng, Y. Lei, and P. Song, "Hydraulic retarders for heavy vehicles: Analysis of fluid mechanics and computational fluid dynamics on braking torque and temperature rise," *Int. J. Automot. Technol.*, vol. 18, no. 3, pp. 387–396, Jun. 2017.
[10] H. K. Versteeg and W. Malalasekera, *An Introduction to Computational Fluid Dynamics: The Finite Volume Method*. London, U.K.: Pearson, 2007.
[11] S. Haykin and R. Gwynn, *Neural Networks and Learning Machines*. Beijing, China: China Machine Press, 2009.
[12] H. Bendu, B. B. V. L. Deepak, and S. Murugan, "Application of GRNN for the prediction of performance and exhaust emissions in HCCI engine using ethanol," *Energy Convers. Manage.*, vol. 122, pp. 165–173, Aug. 2016.
[13] R. Dhanuskodi, R. Kaliappan, S. Suresh, N. Anantharaman, A. Arunagiri, and J. Krishnaiah, "Artificial neural networks model for predicting wall temperature of supercritical boilers," *Appl. Thermal Eng.*, vol. 90, pp. 749–753, Nov. 2015.
[14] Z. Yao, J. Yao, and W. Sun, "Adaptive RISE control of hydraulic systems with multilayer neural-networks," *IEEE Trans. Ind. Electron.*, vol. 66, no. 11, pp. 8638–8647, Nov. 2019.
[15] M. H. Esfe, M. Afrand, W.-M. Yan, and M. Akbari, "Applicability of artificial neural network and nonlinear regression to predict thermal conductivity modeling of Al_2O_3–water nanofluids using experimental data," *Int. Commun. Heat Mass Transf.*, vol. 66, pp. 246–249, Aug. 2015.
[16] Y. C. Lin, J. Li, M.-S. Chen, Y.-X. Liu, and Y.-J. Liang, "A deep belief network to predict the hot deformation behavior of a ni-based superalloy," *Neural Comput. Appl.*, vol. 29, no. 11, pp. 1015–1023, Jun. 2018.
[17] Y. Çay, A. Çiçek, F. Kara, and S. Sağiroğlu, "Prediction of engine performance for an alternative fuel using artificial neural network," *Appl. Thermal Eng.*, vol. 37, pp. 217–225, May 2012.
[18] G. Daniel, *Principles of Artificial Neural Networks*, vol. 7. Singapore: World Scientific, 2013.
[19] J. Yan, X. Guo, G. Tan, T. Yang, and D. Zhou, "Co-simulation based hydraulic retarder braking control system," SAE Tech. Paper 2009-01-2907, 2009.
[20] G. Lechner and H. Naunheimer, *Automotive Transmissions: Fundamentals, Selection, Design and Application*. Berlin, Germany: Springer, 1999.
[21] H.-P. Zheng, Y.-L. Lei, and P.-X. Song, "Water medium retarders for heavy-duty vehicles: Computational fluid dynamics and experimental analysis of filling ratio control method," *J. Hydrodynamics*, vol. 29, no. 6, pp. 1067–1075, Dec. 2017.
[22] Q. Yan, J. Li, and W. Wei, "Research on effect of working oil temperature for hydraulic torque converter performance using CFD and test," *J. Mech. Eng.*, vol. 50, no. 12, pp. 118–125, 2014.
[23] L. Kong, W. Wei, and Q. Yan, "Application of flow field decomposition and reconstruction in studying and modeling the characteristics of a cartridge valve," *Eng. Appl. Comput. Fluid Mech.*, vol. 12, no. 1, pp. 385–396, Jan. 2018.
[24] L. Tan, H. Xie, H. Chen, and H. Yang, "Structure optimization of conical spool and flow force compensation in a diverged flow cartridge proportional valve," *Flow Meas. Instrum.*, vol. 66, pp. 170–181, Apr. 2019.
[25] H. Mu, W. Wei, L. Kong, Y. Zhao, and Q. Yan, "Braking characteristics integrating open working chamber model and hydraulic control system model in a hydrodynamic retarder," *Proc. Inst. Mech. Eng., C, J. Mech. Eng. Sci.*, vol. 233, no. 6, pp. 1952–1971, 2019.
[26] Y. Ö. Özgören, S. Çetinkaya, S. Sarıdemir, A. Çiçek, and F. Kara, "Predictive modeling of performance of a helium charged stirling engine using an artificial neural network," *Energy Convers. Manage.*, vol. 67, pp. 357–368, Mar. 2013.
[27] Z. Waszczyszyn, *Neural Networks in the Analysis and Design of Structures*. Vienna, Austria: Springer, 1999.
[28] J. Han and C. Moraga, "The influence of the sigmoid function parameters on the speed of backpropagation learning," in *Proc. Int. Workshop Artif. Neural Netw.* Berlin, Germany: Springer, 1995, pp. 195–201.
[29] S. Haykin, *Neural Networks: A Comprehensive Foundation*, 3rd ed. New York, NY, USA: Macmillan, 1994.
[30] L. Sun, W. Wei, Q. Yan, and H. Jian, "Artificial neural network–based performance modeling of a diesel engine within the whole operating region considering dynamic conditions," *Proc. Inst. Mech. Eng., D, J. Automobile Eng.*, vol. 233, no. 11, pp. 2970–2984, 2018.
[31] W. W. L. Shu-Cheng, Y. Yang, and Y. Qingdong, "A new modeling method for engine dynamic characteristics based on assembled neural networks," *Trans. Beijing Inst. Technol.*, vol. 27, no. 11, pp. 2544–2564, 2017.
[32] A. Kolmogorov, "On the representation of continuous functions of several variables by superposition of continuous functions of one variable and addition," *Doklady Akademii nauk SSSR*, vol. 114, no. 5, pp. 369–373, 1957.
[33] R. Hecht-Nielsen, "Counterpropagation networks," *Appl. Opt.*, vol. 26, no. 23, pp. 4979–4984, 1987.
[34] E. W. Weisstein. (2006). *Correlation Coefficient*. [Online]. Available: https://mathworld.wolfram.com/
[35] T. Chai and R. R. Draxler, "Root mean square error (RMSE) or mean absolute error (MAE)?—Arguments against avoiding RMSE in the literature," *Geoscientific Model Develop.*, vol. 7, no. 3, pp. 1247–1250, Jun. 2014.
[36] J. E. Nash and J. V. Sutcliffe, "River flow forecasting through conceptual models part I—A discussion of principles," *J. Hydrol.*, vol. 10, no. 3, pp. 282–290, Apr. 1970.
[37] K. Fang, D. Mu, S. Chen, B. Wu, and F. Wu, "A prediction model based on artificial neural network for surface temperature simulation of nickel–metal hydride battery during charging," *J. Power Sources*, vol. 208, pp. 378–382, Jun. 2012.
[38] C. M. Bishop, *Neural Networks for Pattern Recognition*. London, U.K.: Oxford Univ. Press, 1995.
[39] S. Winograd, "A new algorithm for inner product," *IEEE Trans. Comput.*, vol. C-17, no. 7, pp. 693–694, Jul. 1968.
[40] Y. Zhu, Q. Zhang, J. Tao, D. Tan, and X. Wang, "Heat characteristics analysis of electro-hydraulic servo valve," *J. Thermal Sci. Eng. Appl.*, vol. 11, no. 3, Jun. 2019, Art. no. 031008.
[41] T. L. Bergman, F. P. Incropera, D. P. DeWitt, and A. S. Lavine, *Fundamentals of Heat and Mass Transfer*. Hoboken, NJ, USA: Wiley, 2011.
[42] K. J. Åström and T. Hägglund, *PID Controllers: Theory, Design, and Tuning*, vol. 2. Research Triangle, NC, USA: Instrument Society of America, 1995.

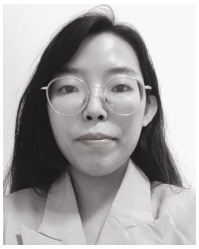

ZHUO WANG received the B.Sc. and M.Eng. degrees in mechanical engineering from Yanshan University, Qinhuangdao, China, in 2013 and 2016, respectively. She is currently pursuing the Ph.D. degree in mechanical engineering with the Beijing Institute of Technology, Beijing, China.

From 2018 to 2019, she was a Visiting Scholar with the Texas A&M University, College Station, TX, USA. Her research interests include modeling and simulation of hydraulic systems, vehicle dynamic and control, and computational fluid dynamic.

WEI WEI received the B.Sc., M.Sc., and Ph.D. degrees from the Beijing Institute of Technology (BIT), Beijing, China, in 2000, 2003, and 2006, respectively.

Since 2006, he has been working with BIT, where he is currently an Associate Professor with the Department of Vehicle Engineering. From 2014 to 2015, he made research as a Research Scholar with the University of Virginia, Charlottesville, VA, USA. His research interests include fluid transmission and controls for vehicles with hydrodynamic components. He has coauthored *Hydrodynamic Components Design* (2015) and *Hydrodynamic Components Three Dimensional Design Optimization* (2017).

Dr. Wei is a committee member of Fluid Transmission and Control Institution of the Chinese Mechanical Engineering Association.

REZA LANGARI (Senior Member, IEEE) received the B.Sc., M.Sc., and Ph.D. degrees from the University of California, Berkeley, CA, USA, in 1981, 1983, and 1991, respectively.

He was with Measurex Corporation from 1984 to 1995, Integrated Systems, Inc., from 1985 to 1986, and Insight Development Corporation from 1987 to 1989, prior to starting his academic career with Texas A&M University, College Station, TX, USA, in 1991. Since then, he has held research positions at the National Aeronautics and Space Administration Ames Research Center, the Rockwell International Science Center, the United Technologies Research Center, and the U.S. Air Force Research Laboratory. He has coauthored *Fuzzy Logic: Intelligence, Control and Information* (Prentice Hall, 1999) and *Measurement and Instrumentation* (Elsevier, 2011, 2015, Second Edition). He has co-edited the *Fuzzy Control: Synthesis and Analysis* (Wiley, 2000) and the *Industrial Applications of Fuzzy Systems* (IEEE Press, 1995). His research interests include in the area of computational intelligence, with application to mechatronic systems, industrial automation, and automated vehicles.

Dr. Langari has served as an Associate Editor for the IEEE TRANSACTIONS ON FUZZY SYSTEMS, the IEEE TRANSACTIONS ON VEHICULAR TECHNOLOGIES, and the *ASME Journal of Dynamic Systems, Measurement, and Control*. He currently serves as the Editor-in-Chief for the *Journal of Intelligent and Fuzzy Systems* (IOS Press, The Netherlands).

QINGYU ZHANG received the B.Sc. and M.Eng. degrees in automotive engineering from Tongji University, Shanghai, China, and the Ph.D. degree in mechanical engineering from Texas A&M University, College Station, TX, USA, in 2011, 2014, and 2019, respectively.

His research interests include automotive engineering, optimal control, and game theory.

QINGDONG YAN received the B.Sc., M.Sc., and Ph.D. degrees in mechanical engineering from the Beijing Institute of Technology (BIT), Beijing, China, in 1985, 1988, and 1995, respectively.

Since 2000, he has been a Professor with BIT, where he is currently the Deputy Director of the Vehicle Engineering Department. His research interests include fluid power transmission and control and vehicle dynamic and control.

Dr. Yan is a Senior Member of the China Mechanical Engineering Society.